

Diluted networks of nonlinear resistors and fractal dimensions of percolation clusters

H. K. Janssen and O. Stenull

Institut für Theoretische Physik III, Heinrich-Heine-Universität, Universitätsstraße 1, 40225 Düsseldorf, Germany

(Received 27 October 1999)

We study random networks of nonlinear resistors, which obey a generalized Ohm's law $V \sim I^r$. Our renormalized field theory, which thrives on an interpretation of the involved Feynman diagrams as being resistor networks themselves, is presented in detail. By considering distinct values of the nonlinearity r , we calculate several fractal dimensions characterizing percolation clusters. For the dimension associated with the red bonds we show that $d_{\text{red}} = 1/\nu$ at least to order $O(\epsilon^4)$, with ν being the correlation length exponent, and $\epsilon = 6 - d$, where d denotes the spatial dimension. This result agrees with a rigorous one by Coniglio. Our result for the chemical distance, $d_{\text{min}} = 2 - \epsilon/6 - [937/588 + 45/49(\ln 2 - 9/10 \ln 3)](\epsilon/6)^2 + O(\epsilon^3)$ verifies a previous calculation by one of us. For the backbone dimension we find $D_B = 2 + \epsilon/21 - 172\epsilon^2/9261 + 2[-74639 + 22680\zeta(3)]\epsilon^3/4084101 + O(\epsilon^4)$, where $\zeta(3) = 1.202057\cdots$, in agreement to second order in ϵ with a two-loop calculation by Harris and Lubensky.

PACS number(s): 64.60.Ak, 64.60.Fr, 72.80.Ng, 05.70.Jk

I. INTRODUCTION

Percolation is a leading paradigm for disorder (for a review see, e.g., Refs. [1–3]). Though it represents the simplest model of a disordered system, it has many applications, e.g., polymerization, porous and amorphous materials, thin films, spreading of epidemics, etc. In particular the transport properties of percolation clusters have gained a vast amount of interest over the last decades. Random resistor networks (RRNs) play a major role in the study of transport on percolation clusters for several reasons. For example, one can learn about the conductivity of disordered media, which might be important for technical applications. One can study diffusion on disordered substrates, since the diffusion constant D and the conductivity Σ of the system are related by the Einstein relation

$$\Sigma = \frac{e^2 n}{K_B T} D, \quad (1.1)$$

where e and n denote the charge and the density of the mobile particles. Nonlinear RRNs, for which the voltage drop V over an individual resistor depends on some power r of the current I flowing through it, can be exploited to derive the fractal dimension of various substructures of percolation clusters.

In this paper we present in detail our study of nonlinear RRNs by renormalized field theory. A brief account of this work has been given previously in Ref. [4]. It is based on an approach by Stephen [5], its refinements by Harris and Lubensky [6], and its generalization to nonlinear resistors by Harris [7]. Our work thrives on the interpretation of the involved Feynman diagrams as being resistor networks themselves [8,4]. This interpretation leads to a substantial simplification of the field theoretic calculations, as we demonstrate by calculating the fractal dimensions of the chemical length and the backbone to two- and three-loop order, respectively.

II. MODEL

Consider a d -dimensional lattice, where bonds between nearest-neighboring sites are randomly occupied with probability p or empty with probability $1 - p$. Each occupied bond has a finite nonzero conductance σ whereas unoccupied bonds have conductance zero. We suppose that the system is near the percolation threshold, i.e., p is close to the critical concentration p_c above which an infinite cluster exists. We are interested in the resistance $R_r(x, x')$ between two lattice sites x and x' averaged subject to the condition, that x and x' are on the same cluster,

$$M_r = \langle \chi(x, x') R_r(x, x') \rangle_C / \langle \chi(x, x') \rangle_C. \quad (2.1)$$

$\langle \cdots \rangle_C$ denotes the average over all configurations of the diluted lattice and $\chi(x, x')$ is an indicator function that takes the value one if x and x' are on the same cluster and zero otherwise. Note that $\langle \chi(x, x') \rangle_C$ is nothing more than the usual correlation function in percolation theory. At criticality M_r obeys [9,10]

$$M_r \sim |x - x'|^{\phi_r/\nu}, \quad (2.2)$$

where ν is the correlation length exponent defined by $\xi \sim (p - p_c)^{-\nu}$.

A. Kirchhoff's laws

Here, we consider a nonlinear RRN as proposed by Kenkel and Straley [11]. The bonds between nearest-neighboring sites i and j obey a generalized Ohm's Law,

$$V_j - V_i = \rho_{i,j} I_{i,j} |I_{i,j}|^{r-1} \quad (2.3)$$

or, equivalently,

$$\sigma_{i,j} (V_j - V_i) |V_j - V_i|^{s-1} = I_{i,j}, \quad (2.4)$$

where $\sigma_{i,j}(\rho_{i,j})$ is the nonlinear conductance (resistance) of the bond $\langle i, j \rangle$, $I_{i,j}$ is the current flowing through the bond from j to i and V_i is the potential at site i . The exponents r

and s are describing the non linearity with $r=s^{-1}$. The conductance and the resistance are related via $\sigma_{i,j}=\rho_{i,j}^{-s}$.

Suppose a current I is put into a cluster at site x and taken out at site x' . Those sites connected to x and x' by mutually avoiding paths are constituting the backbone between x and x' . The power dissipated on the backbone is by definition

$$P=I(V_x-V_{x'}). \quad (2.5)$$

Using Ohm's law, it may be expressed entirely in terms of voltages as

$$\begin{aligned} P &= R_r(x,x')^{-1} |V_x - V_{x'}|^{s+1} \\ &= \sum_{\langle i,j \rangle} \sigma_{i,j} |V_i - V_j|^{s+1} = P(\{V\}), \end{aligned} \quad (2.6)$$

where the sum is taken over all nearest neighbor pairs on the cluster and $\{V\}$ denotes the corresponding set of voltages. As a consequence of the variation principle

$$\frac{\partial}{\partial V_i} \left[\frac{1}{s+1} P(\{V\}) - \sum_j I_j V_j \right] = 0, \quad (2.7)$$

one obtains the circuit equations

$$\sum_{\langle j \rangle} \sigma_{i,j} (V_i - V_j) |V_i - V_j|^{s-1} = - \sum_{\langle j \rangle} I_{i,j} = I_i, \quad (2.8)$$

where $I_i = I(\delta_{i,x} - \delta_{i,x'})$ and the summations extend over the nearest neighbors of i .

Alternatively to Eq. (2.6) the power can be rewritten in terms of the currents as

$$P = R_r(x,x') |I|^{r+1} = \sum_{\langle i,j \rangle} \rho_{i,j} |I_{i,j}|^{r+1} = P(\{I\}), \quad (2.9)$$

with $\{I\}$ denoting the set of currents flowing through the individual bonds. Obviously the cluster may contain closed loops as subnetworks. Suppose there are currents $\{I^{(l)}\}$ circulating independently around a complete set of independent closed loops. Then the power is not only a function of I but also of the set of loop currents. The potential drop around closed loops is zero. This gives rise to the variation principle

$$\frac{\partial}{\partial I^{(l)}} P(\{I^{(l)}\}, I) = 0. \quad (2.10)$$

Equation (2.10) may be used to eliminate the loop currents and thus provides us with a method to determine the total resistance of the backbone via Eq. (2.9).

B. Connection to cluster properties

Here we provide background on the meaning of ϕ_r for some specific values of r . For $r \rightarrow 1$, one recovers the linear RRN. ϕ_1 is the usual resistance exponent as studied to order ϵ^2 , e.g., in Ref. [8].

Other values of r are related to the fractal dimension of substructures of percolation clusters. Consider $r \rightarrow -1^+$. One obtains immediately as a consequence of Eq. (2.9), that

$$R_{-1}(x,x') = \lim_{r \rightarrow -1^+} \sum_{\langle i,j \rangle} \rho_{i,j} \left| \frac{I_{i,j}}{I} \right|^{r+1} = \sum_{\langle i,j \rangle} \rho_{i,j}, \quad (2.11)$$

with only those bonds carrying nonzero current contributing to the sum on the right-hand side. Hence

$$M_{-1}(x,x') \sim M_B, \quad (2.12)$$

where M_B stands for the number of bonds belonging to the backbone. Thus, the fractal dimension of the backbone can be expressed as

$$D_B = \lim_{r \rightarrow -1^+} \phi_r / \nu. \quad (2.13)$$

Now we turn to $r \rightarrow \infty$ and $r \rightarrow 0^+$ following the lines of Blumenfeld and Aharony [12]. On the backbone between two sites x and x' one may distinguish between two different substructures: blobs formed by multiconnected bonds and singly connected bonds which are referred to as red bonds. Both substructures are contributing to the resistance of the backbone

$$R_r(x,x') = \sum_{\langle i,j \rangle}^{\text{blob}} \rho_{i,j} \left| \frac{I_{i,j}}{I} \right|^{r+1} + \sum_{\langle i,j \rangle}^{\text{red}} \rho_{i,j}, \quad (2.14)$$

where the sums are taken over all bonds belonging to blobs and over all red bonds, respectively. Since sites on a blob are multi-connected by definition $I_{i,j} < I$ and thus

$$\lim_{r \rightarrow \infty} \sum_{\langle i,j \rangle}^{\text{blob}} \rho_{i,j} \left| \frac{I_{i,j}}{I} \right|^{r+1} = 0. \quad (2.15)$$

In conclusion, the dimension of the red bonds is related to ϕ_r via

$$d_{\text{red}} = \lim_{r \rightarrow \infty} \phi_r / \nu. \quad (2.16)$$

Consider now the first site x at some end of a blob. An entering current I splits into currents $I_{i,x}$ flowing to nearest neighbors i with

$$|I_{i,x}| = \sigma_{i,x} |V_x - V_i|^s. \quad (2.17)$$

In the limit $s \rightarrow \infty$ the ratios $|I_{i,x}|/|I_{j,x}|$ vanish whenever $\sigma_{i,x} |V_x - V_i|^s < \sigma_{j,x} |V_x - V_j|^s$. Thus, current flows only through the resistor with the largest $\sigma_{i,x} |V_x - V_i|^s$. This argument may be iterated through the entire blob. One identifies either a single self avoiding chain through which I flows, with

$$P = \sum_{\langle i,j \rangle} \rho_{i,j} |I|^{r+1} \quad (2.18)$$

being the power dissipated on the chain, or several of such chains with identical power. The expression in Eq. (2.18) is minimal for minimal $\sum_{\langle i,j \rangle} \rho_{i,j}$, i.e., the current chooses the shortest path through the blob and one is led to

$$d_{\min} = \lim_{r \rightarrow 0^+} \phi_r / \nu \quad (2.19)$$

for the chemical length exponent.

C. Generating function

Our aim is to determine M_r . Hence our task is twofold: we need to solve the set of Kirchhoff's equations (2.8) and to perform the average over all configurations of the diluted lattice. It can be accomplished by employing the replica technique [5,6]. The network is replicated D -fold: $V_x \rightarrow \vec{V}_x = (V_x^{(1)}, \dots, V_x^{(D)})$. One introduces

$$\psi_{\vec{\lambda}}(x) = \exp(i\vec{\lambda} \cdot \vec{V}_x), \quad (2.20)$$

where $\vec{\lambda} \cdot \vec{V}_x = \sum_{\alpha} \lambda^{(\alpha)} V_x^{(\alpha)}$ and $\vec{\lambda} \neq \vec{0}$. One considers the correlation function

$$G(x, x'; \vec{\lambda}) = \langle \psi_{\vec{\lambda}}(x) \psi_{-\vec{\lambda}}(x') \rangle_{\text{rep}} \quad (2.21)$$

given by

$$G(x, x'; \vec{\lambda}) = \left\langle Z^{-D} \int \prod_j \prod_{\alpha=1}^D dV_j^{(\alpha)} \exp \left[-\frac{1}{s+1} P(\{\vec{V}\}) + \frac{i\omega}{2} \sum_i \vec{V}_i^2 + i\vec{\lambda} \cdot (\vec{V}_x - \vec{V}_{x'}) \right] \right\rangle_C. \quad (2.22)$$

Here $P(\{\vec{V}\}) = \sum_{\alpha=1}^D P(\{V^{(\alpha)}\}) = \sum_{\alpha=1}^D \sum_{\langle i,j \rangle} \sigma_{i,j} |V_i^{(\alpha)} - V_j^{(\alpha)}|^{s+1}$ and Z is the normalization

$$Z = \int \prod_j dV_j \exp \left[-\frac{1}{s+1} P(\{V\}) + \frac{i\omega}{2} \sum_i V_i^2 \right]. \quad (2.23)$$

Note that we have introduced an additional power term $(i\omega/2) \sum_i \vec{V}_i^2$. This is necessary to give the integrals in Eqs. (2.22) and (2.23) a well defined meaning. Without this term the integrands depend only on voltage differences and the integrals are divergent. Physically the new term corresponds to grounding each lattice site by a capacitor of unit capacity. The original situation may be restored by taking the limit of vanishing frequency $\omega \rightarrow 0$.

In contrast to the linear network, P is not quadratic and hence the integration over the voltages is not Gaussian. This obstacle may be surmounted by employing the saddle point method [7]. The saddle point equation is identical to the variation principle stated in Eq. (2.7). Thus the maximum of the integrand is determined by the solution of the circuit equations (2.8) and, up to an unimportant multiplicative constant which goes to one in the limit $D \rightarrow 0$,

$$G(x, x'; \vec{\lambda}) = \left\langle \exp \left(\frac{\Lambda_r(\vec{\lambda})}{r+1} R_r(x, x') \right) \right\rangle_C, \quad (2.24)$$

where

$$\Lambda_r(\vec{\lambda}) = \sum_{\alpha=1}^D (-i\lambda^{(\alpha)})^{r+1}. \quad (2.25)$$

Consequently, $G(x, x'; \vec{\lambda})$ may serve as a generating function for M_r , which may be obtained by taking the derivative of

$$G(x, x'; \vec{\lambda}) = \langle \chi(x, x') \rangle_C \left(1 + \frac{\Lambda_r(\vec{\lambda})}{r+1} M_r(x, x') + \dots \right), \quad (2.26)$$

with respect to Λ_r evaluated at $\vec{\lambda}^2 = 0$.

At this point a comment on the nature of $\vec{\lambda}$ is appropriate. One sets

$$\lambda^{(\alpha)} = i\lambda_0 + \xi^{(\alpha)}, \quad (2.27)$$

with real positive λ_0 and $\xi^{(\alpha)}$ and imposes the condition $\sum_{\alpha=1}^D \xi^{(\alpha)} = 0$. The saddle point approximation in Eq. (2.24) may be justified by demanding

$$\lambda_0 \gg 1. \quad (2.28)$$

On the other hand, substitution of Eq. (2.27) into the definition of Λ_r leads to

$$\begin{aligned} \Lambda_r(\vec{\lambda}) &= \sum_{\alpha=1}^D \left\{ \lambda_0^{r+1} - i(r+1)\lambda_0^r \xi^{(\alpha)} \right. \\ &\quad \left. - \frac{r(r+1)}{2} \lambda_0^{r-1} \xi^{(\alpha)2} + \dots \right\} \\ &= D\lambda_0^{r+1} - \frac{r(r+1)}{2} \lambda_0^{r-1} \bar{\xi}^2 + \dots \end{aligned} \quad (2.29)$$

Thus one can justify the expansion in Eq. (2.26) by invoking the conditions

$$\lambda_0^{r+1} \ll D^{-1} \quad \text{and} \quad \lambda_0^{r-1} \bar{\xi}^2 \ll 1. \quad (2.30)$$

Note that the replica limit $D \rightarrow 0$ allows for a simultaneous fulfilment of the conditions (2.28) and (2.30). However, we will not only rely on these conditions on $\vec{\lambda}$. We will provide several consistency checks for the validity of Harris' saddle point approach as we go along and reproduce known results.

D. Field theoretic Hamiltonian

Since infinite voltage drops between different clusters may occur, it is not guaranteed that Z stays finite, i.e., the limit $\lim_{D \rightarrow 0} Z^D$ is not well defined. Moreover, $\vec{\lambda} = \vec{0}$ has to be excluded properly. Both problems can be handled by resorting to a lattice regularization of the integrals in Eqs. (2.22) and (2.23). One switches to voltage variables $\vec{\theta} = \Delta \vec{\theta} \vec{k}$ taking discrete values on a D -dimensional torus, i.e., \vec{k} is chosen to be a D -dimensional integer with $-M < k^{(\alpha)} \leq M$ and $k^{(\alpha)} = k^{(\alpha)} \bmod(2M)$. In this discrete picture there are $(2M)^D - 1$ independent state variables per lattice site and one can introduce the Potts spins [13]

$$\Phi_{\vec{\theta}}(x) = (2M)^{-D} \sum_{\lambda \neq 0} \exp(i\vec{\lambda} \cdot \vec{\theta}) \psi_{\vec{\lambda}}(x) = \delta_{\vec{\theta}, \vec{\theta}_x} - (2M)^{-D} \quad (2.31)$$

subject to the condition $\sum_{\vec{\theta}} \vec{\theta} \Phi_{\vec{\theta}}(x) = 0$.

Now we revisit Eq. (2.22). Carrying out the average over the diluted lattice configurations provides us with the weight $\exp(-H_{\text{rep}})$ of the average $\langle \dots \rangle_{\text{rep}}$,

$$\begin{aligned} H_{\text{rep}} &= -\ln \left\langle \exp \left(-\frac{1}{s+1} P(\{\vec{\theta}\}) + \frac{i\omega}{2} \sum_i \vec{\theta}_i^2 \right) \right\rangle_C \\ &= -\sum_{\langle i,j \rangle} \ln \left\langle \exp \left(-\frac{1}{s+1} \sigma_{i,j} |\theta_i - \theta_j|^{s+1} \right) \right\rangle_C \\ &\quad - \frac{i\omega}{2} \sum_i \vec{\theta}_i^2, \end{aligned} \quad (2.32)$$

where we have introduced the abbreviation $|\theta|^{s+1} = \sum_{\alpha=1}^D |\theta^{(\alpha)}|^{s+1}$. By dropping a constant term $N_B \ln(1-p)$, with N_B being the number of bonds in the undiluted lattice, one obtains

$$\begin{aligned} H_{\text{rep}} &= -\sum_{\langle i,j \rangle} K(\vec{\theta}_i - \vec{\theta}_j) - \sum_i h(\vec{\theta}_i) \\ &= -\sum_{\langle i,j \rangle} \sum_{\vec{\theta}, \vec{\theta}'} K(\vec{\theta} - \vec{\theta}') \Phi_{\vec{\theta}}(i) \Phi_{\vec{\theta}'}(j) \\ &\quad - \sum_i \sum_{\vec{\theta}} h(\vec{\theta}) \Phi_{\vec{\theta}}(i), \end{aligned} \quad (2.33)$$

where

$$K(\vec{\theta}) = \ln \left[1 + \frac{p}{1-p} \exp \left(-\frac{1}{s+1} \sigma |\theta|^{s+1} \right) \right] \quad (2.34)$$

and

$$h(\vec{\theta}) = \frac{i\omega}{2} \vec{\theta}^2. \quad (2.35)$$

Note that $K(\vec{\theta})$ is an exponentially decreasing function in replica space with a decay rate proportional to σ^{-1} . For large σ , the Hamiltonian H_{rep} describes a translationally invariant short range interaction of Potts spins in real and replica space with an external one site potential $h(\vec{\theta})$. Moreover, the interaction potential $K(\vec{\theta})$ is an analytic function of $\sum_{\alpha=1}^D |\theta^{(\alpha)}|^{s+1}$. Thus the Fourier transform

$$\tilde{K}(\vec{\lambda}) = \frac{1}{(2M)^D} \sum_{\vec{\theta}} \exp(-i\vec{\lambda} \cdot \vec{\theta}) K(\vec{\theta}) \quad (2.36)$$

can be Taylor expanded as

$$\tilde{K}(\vec{\lambda}) = w_0 - \sum_{p=1}^{\infty} w_{r,p} [-\Lambda_r(\vec{\lambda})]^p, \quad (2.37)$$

with w_0 and $w_{r,p} \sim \sigma^{-p}$ being expansion coefficients.

In the limit of perfect transport, $\sigma \rightarrow \infty$, $K(\vec{\theta})$ goes to its local limit $K(\vec{\theta}) = K \delta_{\vec{\theta}, \vec{0}}$, with K being a positive constant. The interaction part of the Hamiltonian reduces to

$$H_{\text{rep}}^{\text{int}} = -K \sum_{\langle i,j \rangle} \sum_{\vec{\theta}} \Phi_{\vec{\theta}}(i) \Phi_{\vec{\theta}}(j). \quad (2.38)$$

This represents nothing more than the $(2M)^D$ states Potts model which is invariant against all $(2M)^D!$ permutations of the Potts spins $\Phi_{\vec{\theta}}$. If $\sigma^{-1} \neq 0$, this $S_{(2M)^D}$ symmetry is lost in favor of the short range interaction.

We proceed with the usual coarse graining step and replace the Potts spins $\Phi_{\vec{\theta}}(x)$ by order parameter fields $\varphi(\mathbf{x}, \vec{\theta})$ which inherit the constraint $\sum_{\vec{\theta}} \varphi(\mathbf{x}, \vec{\theta}) = 0$. We model the corresponding field theoretic Hamiltonian \mathcal{H} in the spirit of Landau as a mesoscopic free energy from local monomials of the order parameter field and its gradients in real and replica space. The gradient expansion is justified since the interaction is short ranged in both spaces. Purely local terms in replica space have to respect the full $S_{(2M)^D}$ Potts symmetry. After these remarks we write down the Landau-Ginzburg-Wilson type Hamiltonian

$$\begin{aligned} \mathcal{H} &= \int d^d x \sum_{\vec{\theta}} \left\{ \frac{\tau}{2} \varphi(\mathbf{x}, \vec{\theta})^2 - \frac{w_r}{2} \varphi(\mathbf{x}, \vec{\theta}) \right. \\ &\quad \times \sum_{\alpha=1}^D \left(-\frac{\partial}{\partial \theta^{(\alpha)}} \right)^{r1} \varphi(\mathbf{x}, \vec{\theta}) + \frac{1}{2} [\nabla \varphi(\mathbf{x}, \vec{\theta})]^2 \\ &\quad \left. + \frac{g}{6} \varphi(\mathbf{x}, \vec{\theta})^3 + \frac{i\omega}{2} \vec{\theta}^2 \varphi(\mathbf{x}, \vec{\theta}) \right\}. \end{aligned} \quad (2.39)$$

Here we have neglected all terms that are irrelevant in the renormalization group sense. τ and w_r are now coarse grained analogues of the original coefficients w_0 and $w_{r,1}$ appearing in Eq. (2.37). Terms associated with $w_{r,p}$ are irrelevant for $p \geq 2$ and therefore neglected. Note again that \mathcal{H} reduces to the usual $(2M)^D$ states Potts model Hamiltonian by setting $w_r = 0$ as one retrieves purely geometrical percolation in the limit of vanishing w_r ($\sigma \rightarrow \infty$).

III. RENORMALIZATION GROUP ANALYSES

A. Resistance of Feynman diagrams

The diagrammatic elements contributing to our renormalization group improved perturbation calculation are the three point vertex $-g$ and the propagator

$$\frac{1 - \delta_{\vec{\lambda}, \vec{0}}}{\mathbf{p}^2 + \tau - w_r \Lambda_r(\vec{\lambda})} = \frac{1}{\mathbf{p}^2 + \tau - w_r \Lambda_r(\vec{\lambda})} - \frac{\delta_{\vec{\lambda}, \vec{0}}}{\mathbf{p}^2 + \tau}. \quad (3.1)$$

Note that we have switched to a $(\mathbf{p}, \vec{\lambda})$ representation by employing Fourier transformation in real and replica space. Equation (3.1) shows that the principal propagator decomposes into a propagator carrying $\vec{\lambda}$'s (conducting) and one not carrying $\vec{\lambda}$'s (insulating). This allows for a schematic decomposition of principal diagrams into sums of diagrams consisting of conducting and insulating propagators (see Appendix A). Here a new interpretation of the Feynman diagrams emerges [8]. They may be viewed as resistor networks themselves with conducting propagators corresponding to conductors and insulating propagators corresponding to open

bonds. The parameters s appearing in a Schwinger parametrization of the conducting propagators

$$\frac{1}{\mathbf{p}^2 + \tau - w_r \Lambda_r(\vec{\lambda})} = \int_0^\infty ds \exp\{-s[\tau + \mathbf{p}^2 - w_r \Lambda_r(\vec{\lambda})]\}, \quad (3.2)$$

correspond to resistances and the replica variables $i\vec{\lambda}$ to currents. The replica currents are conserved in each vertex and we may write for each edge i of a diagram $\vec{\lambda}_i = \vec{\lambda}_i(\vec{\lambda}, \{\vec{\kappa}\})$, where $\vec{\lambda}$ is an external current and $\{\vec{\kappa}\}$ denotes a complete set of independent loop currents. The $\vec{\lambda}$ -dependent part of a diagram can be expressed in terms of its power P :

$$\exp\left(w_r \sum_i s_i \Lambda_r(\vec{\lambda})\right) = \exp[w_r P(\vec{\lambda}, \{\vec{\kappa}\})]. \quad (3.3)$$

The new interpretation suggests an alternative way of computing the Feynman diagrams. To evaluate sums over independent loop currents

$$\sum_{\{\kappa\}} \exp[w_r P(\vec{\lambda}, \{\vec{\kappa}\})] \quad (3.4)$$

we employ the saddle point method under the conditions discussed at the end of Sec. II C. Note that the saddle point equation is nothing more than the variation principle stated in Eq. (2.10). Thus solving the saddle point equations is equivalent to determining the total resistance $R_r(\{s_i\})$ of a diagram, and the saddle point evaluation of Eq. (3.4) yields

$$\exp[R_r(\{s_i\})w_r \Lambda_r(\vec{\lambda})], \quad (3.5)$$

where we have omitted once more multiplicative factors which go to one for $D \rightarrow 0$. A completion of squares in the momenta renders the momentum integrations straightforward. Equally well we can use the saddle point method which is exact here since the momentum dependence is purely quadratic. After an expansion for small $\Lambda_r(\vec{\lambda})$ all diagrammatic contributions are of the form

$$\begin{aligned} I(\mathbf{p}^2, \vec{\lambda}^2) &= I_P(\mathbf{p}^2) + I_W(\mathbf{p}^2)w_r \Lambda_r(\vec{\lambda}) + \dots \\ &= \int_0^\infty \prod_i ds_i [1 + R_r(\{s_i\})w_i \Lambda_r(\vec{\lambda}) + \dots] \\ &\quad \times D(\mathbf{p}^2, \{s_i\}). \end{aligned} \quad (3.6)$$

$D(\mathbf{p}^2, \{s_i\})$ is nothing more than the integrand one obtains upon Schwinger parametrization of the corresponding diagram in the usual ϕ^3 theory.

B. Renormalization and scaling

We proceed with standard techniques of renormalized field theory [14]. The ultraviolet divergences occurring in the diagrams can be regularized by dimensional regularization. We employ the renormalization scheme

$$\varphi \rightarrow \hat{\varphi} = Z^{1/2} \varphi, \quad \tau \rightarrow \hat{\tau} = Z^{-1} Z_\tau \tau, \quad (3.7a)$$

$$w_r \rightarrow \hat{w}_r = Z^{-1} Z_{w_r} w_r, \quad g \rightarrow \hat{g} = Z^{-3/2} Z_u^{1/2} G_\epsilon^{-1/2} u^{1/2} \mu^{\epsilon/2}, \quad (3.7b)$$

where $\epsilon = 6 - d$ and μ is an inverse length scale. The factor $G_\epsilon = (4\pi)^{-d/2} \Gamma(1 + \epsilon/2)$, with Γ denoting the gamma function, is introduced for convenience. The Z factors may be determined by minimal subtraction, i.e., they are chosen to solely cancel poles in ϵ . Z , Z_τ , and Z_u are the usual Potts model Z factors. They have been computed to three loop order by de Alcantara Bonfim *et al.* [15]. It remains to calculate Z_{w_r} .

The unrenormalized theory has to be independent of the length scale μ^{-1} introduced by renormalization. In particular, the connected N point correlation functions must be independent of μ , i.e.,

$$\mu \frac{\partial}{\partial \mu} \hat{G}_N(\{\mathbf{x}, \hat{w}_r \Lambda_r(\vec{\lambda})\}; \hat{\tau}, \hat{g}) = 0 \quad (3.8)$$

for all N . Equation (3.8) translates via the Wilson functions

$$\beta(u) = \mu \left. \frac{\partial u}{\partial \mu} \right|_0, \quad \kappa(u) = \mu \left. \frac{\partial \ln \tau}{\partial \mu} \right|_0, \quad (3.9a)$$

$$\zeta_r(u) = \mu \left. \frac{\partial \ln w_r}{\partial \mu} \right|_0, \quad \gamma_{\dots}(u) = \mu \left. \frac{\partial}{\partial \mu} \ln Z_{\dots} \right|_0, \quad (3.9b)$$

where the bare quantities are kept fix while taking the derivatives, into the Gell-Mann-Low renormalization group equation

$$\begin{aligned} &\left[\mu \frac{\partial}{\partial \mu} + \beta \frac{\partial}{\partial u} + \tau \kappa \frac{\partial}{\partial \tau} + w_r \zeta_r \frac{\partial}{\partial w_r} + \frac{N}{2} \gamma \right] \\ &\quad \times G_N(\{\mathbf{x}, w_r \Lambda_r(\vec{\lambda})\}; \tau, u, \mu) = 0. \end{aligned} \quad (3.10)$$

The particular form of the Wilson functions can be extracted from the renormalization scheme and the Z factors.

The renormalization group equation is solved by the method of characteristics. At the infrared stable fixed point u^* , determined by $\beta(u^*) = 0$, the solution reads

$$\begin{aligned} &G_N(\{\mathbf{x}, w_r \Lambda_r(\vec{\lambda})\}; \tau, u, \mu) \\ &= l^{\gamma^* N/2} G_N(\{l \mathbf{x}, l^{\zeta_r^*} w_r \Lambda_r(\vec{\lambda})\}; l^{\kappa^*} \tau, u^*, l \mu), \end{aligned} \quad (3.11)$$

where $\gamma^* = \gamma(u^*)$, $\kappa^* = \kappa(u^*)$ and $\zeta_r^* = \zeta_r(u^*)$.

To get a scaling relation for the correlation functions, a dimensional analysis remains to be performed. It yields

$$\begin{aligned} &G_N(\{\mathbf{x}, w_r \Lambda_r(\vec{\lambda})\}; \tau, u, \mu) \\ &= \mu^{(d-2)N/2} G_N(\{\mu \mathbf{x}, \mu^{-2} w_r \Lambda_r(\vec{\lambda})\}; \mu^{-2} \tau, u, 1). \end{aligned} \quad (3.12)$$

From Eqs. (3.11) and (3.12) we drive the scaling relation

$$\begin{aligned}
& G_N(\{\mathbf{x}, w_r \Lambda_r(\vec{\lambda})\}; \tau, u, \mu) \\
&= l^{(d-2+\eta)N/2} G_N(\{l\mathbf{x}, l^{-\phi_r/\nu} w_r \Lambda_r(\vec{\lambda})\}; l^{-1/\nu} \tau, u^*, \mu),
\end{aligned} \tag{3.13}$$

with the well known critical exponents for percolation [15]

$$\begin{aligned}
\eta = \gamma^* &= -\frac{1}{21} \epsilon - \frac{206}{9261} \epsilon^2 \\
&+ \left[-\frac{93619}{8168202} + \frac{256}{7203} \zeta(3) \right] \epsilon^3 + O(\epsilon^4)
\end{aligned} \tag{3.14}$$

and

$$\begin{aligned}
\nu &= (2 - \kappa^*)^{-1} = \frac{1}{2} + \frac{5}{84} \epsilon + \frac{589}{37044} \epsilon^2 \\
&+ \left[\frac{716519}{130691232} - \frac{89}{7203} \zeta(3) \right] \epsilon^3 + O(\epsilon^4).
\end{aligned} \tag{3.15}$$

Note that ζ in Eq. (3.14) stands for the Riemann zeta function and should not be confused with the Wilson function defined above. The exponent ϕ_r is defined by

$$\phi_r = \nu(2 - \zeta_r^*) = \nu(2 - \eta + \psi_r) \tag{3.16}$$

with $\psi_r = \gamma_w(u^*)$. For arbitrary r we find to one-loop order (for details see Appendix B)

$$\phi_r = 1 + \frac{\epsilon}{14} c_r + O(\epsilon^2), \tag{3.17}$$

with

$$c_r = \frac{1}{2} \int_{-1}^1 d\xi \frac{(1 - \xi^2)}{[(1 + \xi)^{1/r} + (1 - \xi)^{1/r}]^r}, \tag{3.18}$$

in conformity with the result by Harris [7]. Calculating ϕ_r for general r to higher loop orders appears to be out of scope. The reason is, that conducting diagrams C appear. The total resistance of these diagrams cannot be determined by using simple rules for adding resistors in series or in parallel [see Eqs. (B1) and (B2)]. Instead, one has to solve the set of nonlinear circuit equations which is not feasible in closed form.

Equation (3.13) implies the following scaling behavior of the two point correlation function $G = G_2$ at criticality,

$$G[|\mathbf{x} - \mathbf{x}'|, w_r \Lambda_r(\vec{\lambda})] = l^{d-2+\eta} G[l|\mathbf{x} - \mathbf{x}'|, l^{-\phi_r/\nu} w_r \Lambda_r(\vec{\lambda})], \tag{3.19}$$

where we dropped several arguments for notational simplicity. The choice $l = |\mathbf{x} - \mathbf{x}'|^{-1}$ and a Taylor expansion of the right hand side of Eq. (3.19) lead to

$$\begin{aligned}
& G[|\mathbf{x} - \mathbf{x}'|, w_r \Lambda_r(\vec{\lambda})] \\
&= |\mathbf{x} - \mathbf{x}'|^{2-d-\eta} [1 + w_r \Lambda_r(\vec{\lambda}) |\mathbf{x} - \mathbf{x}'|^{\phi_r/\nu} + \dots].
\end{aligned} \tag{3.20}$$

Comparison with Eq. (2.26) gives us the scaling behavior of the average resistance:

$$M_r(\mathbf{x}, \mathbf{x}') \sim |\mathbf{x} - \mathbf{x}'|^{\phi_r/\nu}. \tag{3.21}$$

IV. FRACTAL DIMENSIONS

In this section we calculate ϕ_r for $r \rightarrow \infty$, $r \rightarrow 0^+$, and $r \rightarrow -1^+$. As discussed in Sec. II B, this provides us with the fractal dimension of the red bonds, the chemical length, and the backbone, respectively.

A. Red bonds

Consider $r \rightarrow \infty$. As argued in Sec. II B, blobs do not contribute to the total resistance. Now we take direct advantage of our view of the Feynman diagrams as being resistor networks themselves. In analogy to real networks, the resistance of closed loops vanishes. Only singly connected conducting propagators contribute to the total resistance of a diagram, i.e.,

$$R_\infty(\{s_i\}) = \sum_i^{\text{singly}} s_i, \tag{4.1}$$

with the sum being taken only over singly connected conducting propagators. The contribution of a diagram to the renormalization factor Z_{w_∞} takes the form

$$I_W(\mathbf{p}^2) = \int_0^\infty \prod_j ds_j \sum_i^{\text{singly}} s_i D(\mathbf{p}^2, \{s_j\}). \tag{4.2}$$

Note that a factor s_i in Eq. (4.2) corresponds to the insertion of $\frac{1}{2} \varphi^2$ into the i th edge of the diagram. We generate $I_W(\mathbf{p}^2)$ by inserting $\frac{1}{2} \varphi^2$ in each singly connected conducting propagator. This procedure is carried out up to three loop order, i.e., every conducting propagator in Appendix A that does not belong to a closed loop gets an insertion. For details see Appendix C. The resulting diagrams are displayed in Fig. 1.

Now consider the contributions of the diagrams listed in Appendix A to Z_τ . These can be generated by inserting $\frac{1}{2} \varphi^2$ in conducting as well as in insulating propagators. Again, one obtains the diagrams depicted in Fig. 1 with the same fore-factors. Consequently, Z_{w_∞} and Z_τ are identical at least up to three-loop order. The same goes for the corresponding Wilson functions ζ_∞ and κ . From the definition of ϕ_r it follows that

$$\phi_\infty = \frac{2 - \zeta_\infty^*}{2 - \kappa^*} = 1 + O(\epsilon^4). \tag{4.3}$$

Note that this result is in agreement with the rigorous one by Coniglio [16,17], who proved that $d_{\text{red}} = 1/\nu$. We rate this as an indication for the validity of Harris' saddle point approach.

B. Chemical length

In the limit $r \rightarrow 0^+$ only the shortest self avoiding path of conducting propagators contributes to the total resistance of a diagram. In other words, the total resistance has to be determined such that

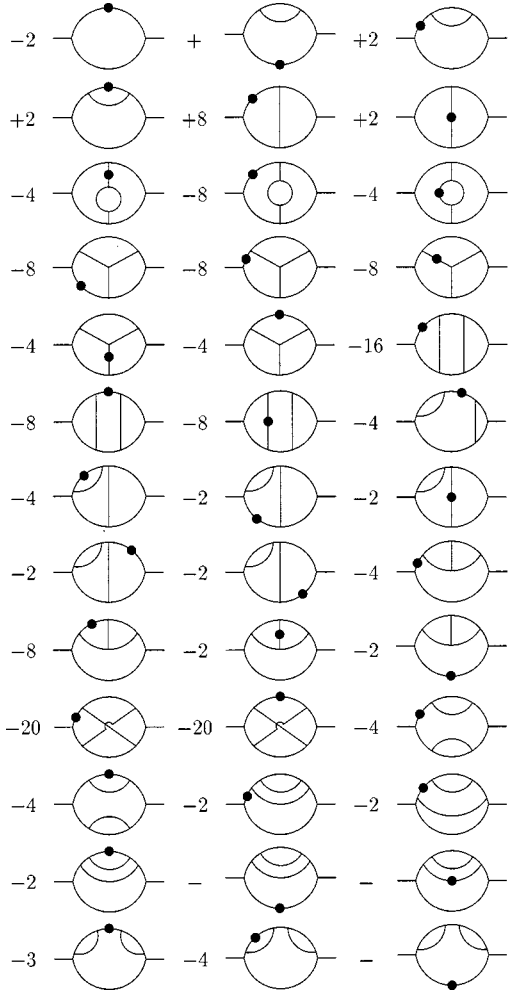


FIG. 1. Diagrammatic expansion in the limit $r \rightarrow \infty$. The listed diagrams including their fore factors can be obtained from the conducting diagrams shown in Appendix A in two different ways: first, connected conducting propagators and secondly, by inserting $\frac{1}{2}\varphi^2$ into every conducting and insulating propagator. As a consequence, the renormalization factors Z_{w_∞} and Z_τ are identical. The lines stand for conducting propagators evaluated at zero currents, the solid dots for $\frac{1}{2}\varphi^2$ insertions.

$$\sum_{\text{paths}} \sum_{i \in \text{path}} s_i \quad (4.4)$$

is minimal, where the first sum is taken over all self-avoiding paths of conducting propagators connecting the external legs of a diagram.

For $r \rightarrow 0^+$ the conducting propagator reads

$$\frac{1}{\tau + \mathbf{p}^2 + iw_0 \sum_{\alpha=1}^D \lambda^{(\alpha)}} = \frac{1}{\chi + iw_0 \lambda}, \quad (4.5)$$

with $\chi = \tau + \mathbf{p}^2$ and $\lambda = \sum_{\alpha=1}^D \lambda^{(\alpha)}$. We start with the two one-loop diagrams A and B (see Appendix A). The diagram A translates into

$$\begin{aligned} A &= \frac{g^2}{2} \int_{\mathbf{p}} \int_0^\infty ds_1 ds_2 \exp[s_1 \chi_1 + s_2 \chi_2] \\ &\quad \times \exp[-iw_0 \lambda \min(s_1, s_2)] \\ &= g^2 \int_{\mathbf{p}} \int_0^\infty ds_1 ds_2 \exp[s_1 \chi_1 + s_2 \chi_2] \\ &\quad \times \exp[-iw_0 \lambda s_1] \theta(s_2 - s_1), \end{aligned} \quad (4.6)$$

where θ denotes the step function and $\int_{\mathbf{p}}$ is an abbreviation for $(2\pi)^{-d} \int d^d p$. Diagram B reads

$$B = \frac{g^2}{2} \int_{\mathbf{p}} \int_0^\infty ds_1 ds_2 \exp[s_1 \chi_1 + s_2 \chi_2] \exp[-iw_0 \lambda s_1], \quad (4.7)$$

and hence,

$$\begin{aligned} A - 2B &= -g^2 \int_{\mathbf{p}} \int_0^\infty ds_1 ds_2 \exp[s_1 \chi_1 + s_2 \chi_2] \\ &\quad \times \exp[-iw_0 \lambda s_1] \theta(s_1 - s_2). \end{aligned} \quad (4.8)$$

Now we take a short detour and present some features of the field theory of dynamical percolation as studied by one of us some time ago [18]. The dynamical functional \mathcal{J} that leads to the diagrammatic expansion for the calculation of correlation and response functions is given by

$$\mathcal{J} = \int d^d x dt \gamma \bar{\varphi} \left[\gamma^{-1} \frac{\partial}{\partial t} + (\tau - \Delta) + g \phi - \frac{g}{2} \bar{\varphi} \right] \varphi. \quad (4.9)$$

Here, $\phi(\mathbf{x}, t) = \gamma \int_{-\infty}^t dt' \varphi(\mathbf{x}, t')$ and $\bar{\varphi}(\mathbf{x}, t)$ is the response field.

$$G_{1,1}(\mathbf{x}, t) = \langle \varphi(\mathbf{x}, t) \bar{\varphi}(\mathbf{0}, t) \rangle_{\mathcal{J}} \quad (4.10)$$

is the density response function that describes a growing cluster initiated by a germ at $(\mathbf{x} = \mathbf{0}, t = 0)$ which percolates at the critical point. Near this percolation point the response function scales as

$$G_{1,1}(\mathbf{x}, t) = \xi^{-(d-2+\eta)} f(\mathbf{x}/\xi, t/\xi^z), \quad (4.11)$$

where f is a scaling function, $\xi = |\tau|^{-\nu}$ is the correlation length, and z is the dynamic exponent given to second order in ϵ in Ref. [18].

The diagrammatic elements of dynamical percolation are the propagator

$$G(\mathbf{p}, t) = \theta(t) \exp[-\gamma(\tau + \mathbf{p}^2)t] \quad (4.12)$$

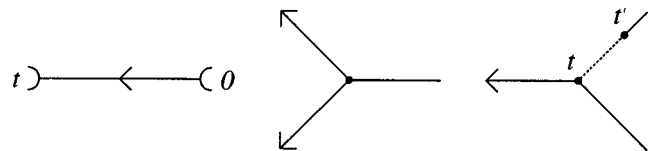


FIG. 2. The propagator $G(\mathbf{p}, t)$ as well as the vertices γg and $-\gamma g \theta(t - t')$ (from left to right).

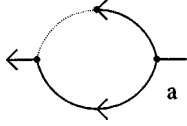


FIG. 3. In the limit $r \rightarrow 0^+$ we map the bold one-loop diagram (see Appendix A) onto the dynamic one shown here. The meaning of the graphic elements may be inferred from Fig. 2.

and the vertices γg and $-\gamma g \theta(t-t')$. These elements are depicted in Fig. 2. Note that the Fourier transformed propagator reads

$$\tilde{G}(\mathbf{p}, \omega) = \frac{1}{i\omega + \gamma(\tau + \mathbf{p}^2)} \quad (4.13)$$

and can be identified with Eq. (4.5) up to a factor γ^{-1} by setting $\gamma w_0 \lambda = \omega$. Thus, the renormalization of w_0 is directly related to that of the kinetic coefficient γ . One finds that z is related to the chemical length dimension by $z = d_{\min}$.

The one loop contribution to the vertex function $\Gamma_{1,1}(\mathbf{p}, \omega) = 1/\tilde{G}_{1,1}(\mathbf{p}, \omega)$ is visualized in Fig. 3. We find

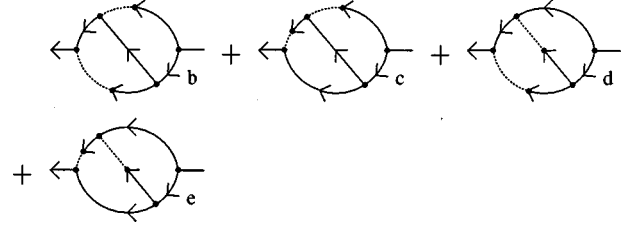


FIG. 4. Dynamic diagrams obtained in the limit $r \rightarrow 0^+$.

$$\begin{aligned} a &= -(\gamma g)^2 \int_{\mathbf{p}} \int_0^\infty dt_1 dt_2 \exp[\gamma(t_1 \chi_1 + t_2 \chi_2)] \theta(t_1 - t_2) \\ &\quad \times \exp[-i\omega t_1] \\ &= A - 2B \end{aligned} \quad (4.14)$$

if we identify $\gamma t_i = s_i$.

Now we turn to the two-loop diagrams. In the same manner as in the one-loop case we obtain

$$\begin{aligned} C - 4D - E + 2F + 4G &= g^4 \int_{\mathbf{p}} \int_{\mathbf{q}} \int_0^\infty \prod_{i=1}^5 ds_i \exp\left(\sum_{i=1}^5 s_i \chi_i\right) \left\{ \exp[-i w_0 \lambda (s_1 + s_4 + s_5)] \{ \theta(s_2 - s_1 - s_5) \theta(s_3 - s_4 - s_5) - \theta(s_2 \right. \\ &\quad \left. - s_1 - s_5) - \theta(s_3 - s_4 - s_5) + 1 \} + \exp[-i w_0 \lambda (s_1 + s_3)] \{ \theta(s_2 + s_4 - s_1 - s_3) \right. \\ &\quad \left. \times \theta(s_4 + s_5 - s_3) \theta(s_2 + s_5 - s_1) - \theta(s_2 + s_4 - s_1 - s_3) - \theta(s_4 + s_5 - s_3) - \theta(s_2 + s_5 - s_1) + 2 \} \right\} \\ &= (\gamma g)^4 \int_{\mathbf{p}} \int_{\mathbf{q}} \int_0^\infty \prod_{i=1}^5 dt_i \exp\left(\sum_{i=1}^5 t_i \gamma \chi_i\right) \left\{ \exp[-i\omega(t_1 + t_4 + t_5)] \theta(t_1 + t_5 - t_2) \theta(t_4 + t_5 - t_3) + \exp \right. \\ &\quad \left. [-i\omega(t_1 + t_3)] \{ \theta(t_1 - t_2 - t_5) \theta(t_3 + t_5 - t_4) + \theta(t_1 + t_3 - t_2 - t_4) [\theta(t_4 - t_3 - t_5) \right. \\ &\quad \left. + \theta(t_3 - t_4 - t_5)] \} \right\} \\ &= b + c + d + e. \end{aligned} \quad (4.15)$$

The diagrams b, c, d, and e are depicted in Fig. 4. For the second bold two-loop diagram we find

$$\begin{aligned} H - I - 2J + 2K + L &= g^4 \int_{\mathbf{p}} \int_{\mathbf{q}} \int_0^\infty \prod_{i=1}^5 ds_i \exp\left(\sum_{i=1}^5 s_i \chi_i\right) \left\{ \exp[-i w_0 \lambda (s_1 + s_2 + s_3)] \{ \theta(s_5 - s_1 - s_2 - s_3) \theta(s_4 - s_2) \right. \\ &\quad \left. - \theta(s_5 - s_1 - s_2 - s_3) - \theta(s_4 - s_2) + 1 \} + \exp[-i w_0 \lambda s_5] \frac{1}{2} \{ \theta(s_1 + s_2 + s_3 - s_5) \theta(s_1 + s_4 + s_3 - s_5) \right. \\ &\quad \left. - \theta(s_1 + s_2 + s_3 - s_5) - \theta(s_1 + s_4 + s_3 - s_5) + 1 \} \right\} \\ &= (\gamma g)^4 \int_{\mathbf{p}} \int_{\mathbf{q}} \int_0^\infty \prod_{i=1}^5 dt_i \exp\left(\sum_{i=1}^5 t_i \gamma \chi_i\right) \left\{ \exp[-i\omega(t_1 + t_2 + t_3)] \theta(t_2 - t_4) \theta(t_1 + t_2 + t_3 - t_5) \right. \\ &\quad \left. + \exp[-i\omega t_5] \theta(t_5 - t_1 - t_2 - t_3) \theta(t_2 - t_4) \right\} \\ &= f + g. \end{aligned} \quad (4.16)$$

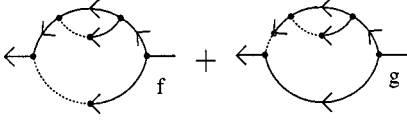


FIG. 5. Dynamic diagrams obtained in the limit $r \rightarrow 0^+$.

The diagrams f and g are shown in Fig. 5.

The dynamic diagrams lead to the result for the dynamic exponent z stated in Ref. [18]. Since we identified the two diagrammatic expansions up to two-loop order, the RRN gives the same result for the chemical length dimension as the dynamic approach in Ref. [18],

$$d_{\min} = 2 - \frac{\epsilon}{6} - \left[\frac{937}{588} + \frac{45}{49} \left(\ln 2 - \frac{9}{10} \ln 3 \right) \right] \left(\frac{\epsilon}{6} \right)^2 + O(\epsilon^3). \quad (4.17)$$

Moreover, another consistency check for the saddle point approximation is fulfilled.

Obviously, d_{\min} has to approach one for $d \rightarrow 1$. This feature can be incorporated by a rational approximation yielding

$$d_{\min} \approx 1 + \left(1 - \frac{\epsilon}{5} \right) \left(1 + \frac{\epsilon}{30} - 0.0301 \epsilon^2 \right). \quad (4.18)$$

Due to the rich structure of η in the percolation problem

$$\psi_0 = -\frac{3}{14} \epsilon - \frac{365 + 140 \ln 2 - 126 \ln 3}{5488} \epsilon^2 \quad (4.19)$$

might be better suited for such a comparison than d_{\min} . It is known exactly that ψ_0 vanishes in one dimension. A rational approximation yields

$$\psi_0 \approx \left(1 - \frac{\epsilon}{5} \right) \left(-\frac{3}{14} \epsilon - 0.1018 \epsilon^2 \right). \quad (4.20)$$

d_{\min} and ψ_0 are compared to numerical simulations by Grassberger [19] in Fig. 6. The rational approximants agree reasonably well with the numerical estimates at $d=3$. At $d=2$, the approximant for d_{\min} seems to be in conformity with the simulation result. However, the good agreement should be taken with caution. It might be accidental, since $\psi_0(d=2)$ hardly agrees with the numerical value.

C. Backbone

Now we focus on the limit $r \rightarrow -1^+$. As argued in Sec. II B, the resistance of the backbone between two sites x and x' is given by

$$R_{-1}(x, x') = \sum_{\langle i, j \rangle} \rho_{i, j}, \quad (4.21)$$

with the sum running over all current carrying bonds of the underlying cluster. In analogy, the resistance of a Feynman diagram is given by

$$R_{-1}(\{s_i\}) = \sum_i^{\text{cond}} s_i, \quad (4.22)$$

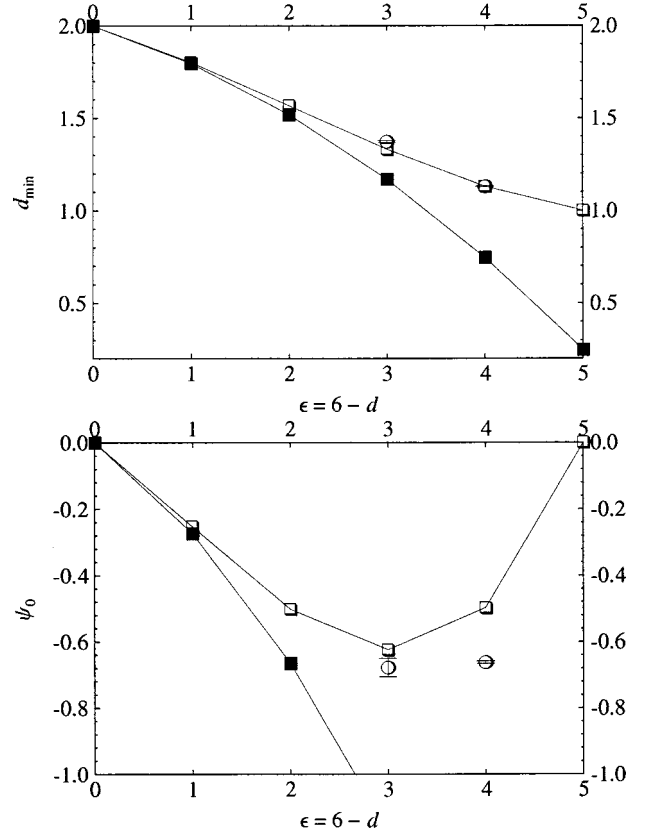


FIG. 6. Dependence of the exponents d_{\min} and $\psi_0 = d_{\min} - \gamma/\nu$ on dimensionality. The ϵ expansion (full squares) and the rational approximation (open squares) are compared to numerical simulations (circles). For d_{\min} we take Monte Carlo results by Grassberger. At $d=2$ we insert the exact values [23,24] $\nu = \frac{4}{3}$ and $\gamma = \frac{43}{18}$. At $d=3$ we use Monte Carlo results by Ziff and Stell [25]: $\nu = 0.875 \pm 0.008$, and $\gamma = 1.795 \pm 0.005$.

where the sum is extending over all conducting propagators of the diagram. The contribution of a diagram to Z_{w-1} now takes the form

$$I_W(\mathbf{p}^2) = \int_0^\infty \prod_j ds_j \sum_i^{\text{cond}} s_i D(\mathbf{p}^2, \{s_j\}). \quad (4.23)$$

We proceed in the same manner as in Sec. IV A. However, now $\frac{1}{2} \phi^2$ is inserted into all conducting propagators. For details of the calculation see Appendix D. Minimal subtraction leads to the renormalization factor

$$Z_{w-1} = 1 + \frac{u^2}{4\epsilon} + \frac{u^3}{\epsilon^2} \left[\frac{7}{12} - \frac{29}{144} \epsilon - \frac{2}{3} \zeta(3) \epsilon \right] + O(u^4). \quad (4.24)$$

Via the Wilson functions we obtain the exponents

$$\psi_{-1} = -2 \left(\frac{\epsilon}{7} \right)^2 + \left[16 \zeta(3) - \frac{2075}{126} \right] \left(\frac{\epsilon}{7} \right)^3 + O(\epsilon^4) \quad (4.25)$$

and

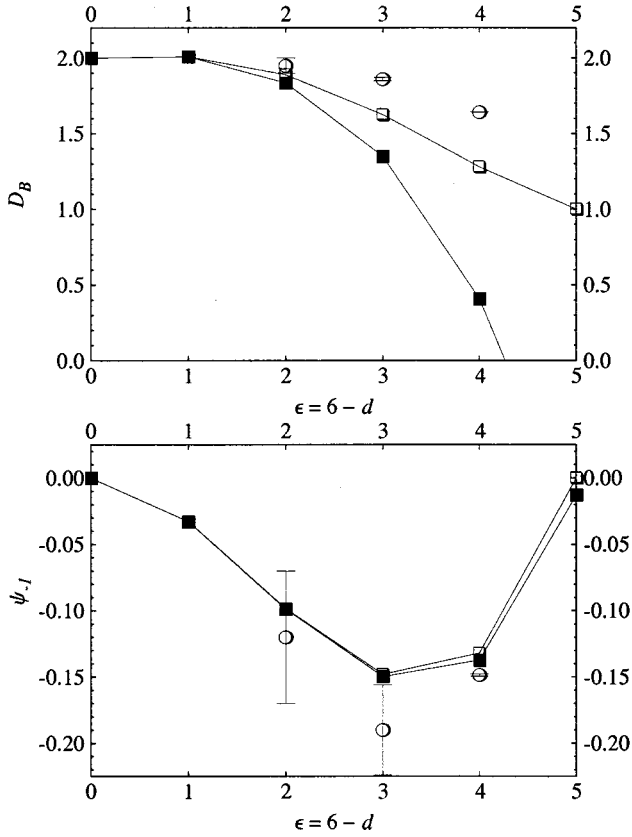


FIG. 7. Dependence of the exponents D_B and $\psi_{-1} = D_B - \gamma/\nu$ on dimensionality. The ϵ expansion (full squares) and the rational approximation (open squares) are compared to numerical results (circles) by Grassberger ($d=2$) and Moukarzel ($d=3,4$). They determined D_B by simulations. At $d=2$ and $d=3$ we use the same values for γ and ν as in Fig. 6. At $d=4$ we take $\nu^{-1} = 1.44 \pm 0.05$ [22] and $\gamma = 1.44$ [2].

$$D_B = 2 + \frac{1}{21} \epsilon - \frac{172}{9261} \epsilon^2 + 2 \frac{-74639 + 22680 \zeta(3)}{4084101} \epsilon^3 + O(\epsilon^4). \quad (4.26)$$

Note that our result agrees to second order in ϵ with calculations by Harris and Lubensky [20] based on another approach. This is again in favor of the saddle point approximation.

In Fig. 7 we compare the ϵ expansions as well as the rational approximants

$$\psi_{-1} \approx -\frac{2\epsilon^2}{49} \left(1 - \frac{\epsilon}{5} \right) \left(1 + 1.2625 \frac{\epsilon}{500} \right) \quad (4.27)$$

and

$$D_B \approx 1 + \left(1 - \frac{\epsilon}{5} \right) \left(1 + \frac{26}{105} \epsilon + \frac{7166}{231525} \epsilon^2 - 0.0170 \epsilon^3 \right) \quad (4.28)$$

to numerical simulations by Grassberger [21] and Moukarzel [22]. At $d=4$ the results agree within the numerical errors. However, a higher accuracy of the numerical estimate is de-

sirable. At $d=3$ and $d=2$ the analytic results look less realistic, but they reproduce the shape of the dependence on dimensionality.

V. CONCLUSIONS AND OUTLOOK

By employing a saddle point approach due to Harris we calculated the exponent ϕ_r/ν for the critical behavior of the resistance in a diluted network. We focussed on distinct values of the nonlinearity r , namely, those related to the fractal dimensions of the red bonds, the chemical path, and the backbone, respectively.

We provided several consistency checks for the saddle point approach. The validity of the approach seems to be beyond question.

For dimensions close to the upper critical dimension six, our results for d_{\min} and D_B are the most accurate analytical estimates that we know of. The analytic results agree reasonably well with the available numerical simulations. At low dimensions the agreement becomes less pronounced.

Our interpretation of Feynman diagrams proved to be a powerful tool. It simplified the renormalization group improved perturbation calculation considerably. The technique used here may be applied to other aspects of transport on percolation clusters. For example, it can be employed to calculate the family of noise exponents $\{\psi_l\}$ for diluted resistor networks, as treated by Park, Harris, and Lubensky [26] to one-loop order. Our two-loop calculation yielding

$$\psi_l = 1 + \frac{\epsilon}{7(1+l)(1+2l)} + \frac{\epsilon^2}{12348(1+l)^3(1+2l)^3} \times \{313 - 672\gamma + l\{3327 - 4032\gamma - 8l\{4(-389 + 273\gamma) + l[-2076 + 1008\gamma + l(-881 + 336\gamma)]\}\} - 672(1+l)^2(1+2l)^2\Psi(1+2l)\} \quad (5.1)$$

will be reported in a separate publication in the near future. In Eq. (5.1) γ denotes Euler's constant and Ψ stands for the Digamma function.

ACKNOWLEDGMENTS

We acknowledge support by the Sonderforschungsbereich 237 "Unordnung und grosse Fluktuationen" of the Deutsche Forschungsgemeinschaft.

APPENDIX A: DECOMPOSITION OF DIAGRAMS

Here we list the decomposition of the primary two leg diagrams (bold) into conducting diagrams composed of conducting (light) and insulating (dashed) propagators. The listing extends up to three-loop order. Note that the conducting diagrams inherit their combinatorial factor from their bold diagram. For example, the diagrams A and B introduced below have to be calculated with the same combinatorial factor, namely, $\frac{1}{2}$.

The diagrammatic equation shows a bold circle with two external legs on the left, followed by an equals sign. To the right of the equals sign are three terms: a light circle with two external legs labeled 'A', followed by a minus sign and the number '2', followed by a dashed circle with two external legs labeled 'B'. The entire equation is labeled (A1) at the bottom right.

$$\begin{aligned}
 & \text{Diagram 1} = \text{Diagram C} - 4 \text{Diagram D} \\
 & - \text{Diagram E} + 2 \text{Diagram F} + 4 \text{Diagram G}
 \end{aligned}
 \tag{A2}$$

$$\begin{aligned}
 & \text{Diagram 1} = \text{Diagram 2} - 4 \text{Diagram 3} \\
 & - 2 \text{Diagram 4} + \text{Diagram 5} + 2 \text{Diagram 6} \\
 & + 8 \text{Diagram 7} - 4 \text{Diagram 8} - 4 \text{Diagram 9}
 \end{aligned}
 \tag{A6}$$

$$\begin{aligned}
 & \text{Diagram 1} = \text{Diagram H} - \text{Diagram I} \\
 & - 2 \text{Diagram J} + 2 \text{Diagram K} + \text{Diagram L}
 \end{aligned}
 \tag{A3}$$

$$\begin{aligned}
 & \text{Diagram 1} = \text{Diagram 2} - \text{Diagram 3} \\
 & - \text{Diagram 4} - \text{Diagram 5} - \text{Diagram 6} \\
 & - 2 \text{Diagram 7} + \text{Diagram 8} + 2 \text{Diagram 9} \\
 & + \text{Diagram 10} + 2 \text{Diagram 11} + 2 \text{Diagram 12} \\
 & + 2 \text{Diagram 13} + 2 \text{Diagram 14} - 2 \text{Diagram 15} \\
 & - 4 \text{Diagram 16} - \text{Diagram 17} - 2 \text{Diagram 18}
 \end{aligned}
 \tag{A7}$$

$$\begin{aligned}
 & \text{Diagram 1} = \text{Diagram 2} - 2 \text{Diagram 3} \\
 & - 2 \text{Diagram 4} - 2 \text{Diagram 5} - \text{Diagram 6} \\
 & - \text{Diagram 7} + 2 \text{Diagram 8} + 2 \text{Diagram 9} \\
 & + 2 \text{Diagram 10} + 4 \text{Diagram 11} + 2 \text{Diagram 12} \\
 & + \text{Diagram 13} + 2 \text{Diagram 14} + 2 \text{Diagram 15} \\
 & + 2 \text{Diagram 16} - 4 \text{Diagram 17} - 2 \text{Diagram 18} \\
 & - 4 \text{Diagram 19} - 4 \text{Diagram 20} - 2 \text{Diagram 21}
 \end{aligned}
 \tag{A4}$$

$$\begin{aligned}
 & \text{Diagram 1} = \text{Diagram 2} - 4 \text{Diagram 3} \\
 & - \text{Diagram 4} - \text{Diagram 5} + 2 \text{Diagram 6} \\
 & + 4 \text{Diagram 7} + 4 \text{Diagram 8} + \text{Diagram 9} \\
 & - 2 \text{Diagram 10} - 2 \text{Diagram 11} - 4 \text{Diagram 12}
 \end{aligned}
 \tag{A8}$$

$$\begin{aligned}
 & \text{Diagram 1} = \text{Diagram 2} - 4 \text{Diagram 3} \\
 & - 2 \text{Diagram 4} - 2 \text{Diagram 5} + 2 \text{Diagram 6} \\
 & + 2 \text{Diagram 7} + 4 \text{Diagram 8} + 8 \text{Diagram 9} \\
 & + \text{Diagram 10} + 4 \text{Diagram 11} - 8 \text{Diagram 12} \\
 & - 2 \text{Diagram 13} - 8 \text{Diagram 14}
 \end{aligned}
 \tag{A5}$$

$$\begin{aligned}
 & \text{Diagram 1} = \text{Diagram 2} - 4 \text{Diagram 3} \\
 & - 4 \text{Diagram 4} + 8 \text{Diagram 5} + 4 \text{Diagram 6} \\
 & + 2 \text{Diagram 7} + 8 \text{Diagram 8} - 16 \text{Diagram 9} \\
 & - 4 \text{Diagram 10}
 \end{aligned}
 \tag{A9}$$

$$(A10)$$

$$(A11)$$

$$(A12)$$

APPENDIX B: ARBITRARY NONLINEARITY

In this appendix we sketch the calculation of ϕ_r for general r to one-loop order. The calculation thrives on the fact that the total resistance of the diagrams A and B can be determined by applying simple rules for resistors added in series or in parallel.

Two nonlinear resistors with resistances ρ_1 and ρ_2 add in series as usual,

$$\rho = \rho_1 + \rho_2. \quad (B1)$$

On the other hand, the total resistance of the two resistors in parallel is given by

$$\rho^{-1/r} = \rho_1^{-1/r} + \rho_2^{-1/r}. \quad (B2)$$

If we Schwinger parametrize the propagators by s_1 and s_2 , the total resistance of diagram A reads

$$R(s_1, s_2) = \frac{s_1 s_2}{[s_1^s + s_2^s]^r}. \quad (B3)$$

For notational simplicity we keep only the part of A proportional to $w_r \Lambda_r(\vec{\lambda})$ and drop all other terms. With Eq. (B3) we have

$$A = -\frac{g^2}{2} w_r \Lambda_r(\vec{\lambda}) \int_0^\infty ds_1 ds_2 \int_{\mathbf{q}} \exp[-(s_1 + s_2) \times (\tau + \mathbf{q}^2)] R(s_1, s_2). \quad (B4)$$

Carrying out the momentum integration gives

$$A = -\frac{g^2}{2} w_r \Lambda_r(\vec{\lambda}) \frac{1}{(4\pi)^{d/2}} \int_0^\infty ds_1 ds_2 \times \exp[-(s_1 + s_2)\tau] \frac{1}{(s_1 + s_2)^{d/2}} \frac{s_1 s_2}{[s_1^s + s_2^s]^r}. \quad (B5)$$

Equation (B5) can be simplified by the change of variables $s_1 \rightarrow t(1 + \xi)$ and $s_2 \rightarrow t(1 - \xi)$. Expansion of the result for small ϵ yields

$$A = -g^2 w_r \Lambda_r(\vec{\lambda}) \frac{G_\epsilon}{\epsilon} \tau^{-\epsilon/2} \times \frac{1}{4} \int_{-1}^1 d\xi \frac{(1 - \xi^2)}{[(1 + \xi)^{1/r} + (1 - \xi)^{1/r}]^r}. \quad (B6)$$

Diagram B is particularly simple to compute. We obtain

$$B = -\frac{g^2}{2} w_r \Lambda_r(\vec{\lambda}) \frac{G_\epsilon}{\epsilon} \tau^{-\epsilon/2}. \quad (B7)$$

Hence the result for the bold diagram composed of A and B is

$$A - 2B = g^2 w_r \Lambda_r(\vec{\lambda}) \frac{G_\epsilon}{\epsilon} \times \tau^{-\epsilon/2} \left\{ 1 - \frac{1}{4} \int_{-1}^1 d\xi \frac{[(1 - \xi^2)]}{[(1 + \xi)^{1/r} + (1 - \xi)^{1/r}]^r} \right\}. \quad (B8)$$

From Eq. (B8) and the renormalization scheme Eq. (3.7) we deduce that

$$Z_{w_r} = 1 + \frac{u}{\epsilon} \left\{ 1 - \frac{1}{4} \int_{-1}^1 d\xi \frac{(1 - \xi^2)}{[(1 + \xi)^{1/r} + (1 - \xi)^{1/r}]^r} \right\}. \quad (B9)$$

The corresponding Wilson function evaluated at the fixed point $u^* = 2\epsilon/7$ reads

$$\psi_r = -\frac{2\epsilon}{7} + \frac{\epsilon}{14} \int_{-1}^1 d\xi \frac{(1 - \xi^2)}{[(1 + \xi)^{1/r} + (1 - \xi)^{1/r}]^r}. \quad (B10)$$

From the definition of ϕ_r , Eq. (3.16), we finally obtain the result stated in Eqs. (3.17) and (3.18).

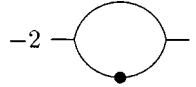
APPENDIX C: DIAGRAMS FOR THE RED BONDS

This appendix gives details on the diagrammatic contributions to the renormalization of w_r and τ in the limit $r \rightarrow \infty$. As an example we consider the one-loop diagrams A and B. In Sec. IV A we argued, that only singly connected conducting propagators contribute to Z_{w_∞} . Thus, A gives no such

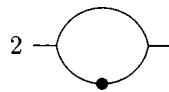
contribution at all. The contribution of B can be expressed as


(C1)

where the lines stand for conducting propagators evaluated at zero currents and the solid dot for an $\frac{1}{2}\phi^2$ insertion. The resulting contribution of A-2B is


(C2)

Now we turn to τ . Z_τ can be calculated by inserting $\frac{1}{2}\phi^2$ into conducting and insulating propagators. The contribution of both A and B reads

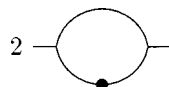

(C3)

The resulting contribution of A-2B is again the one stated in Eq. (C2).

We carry out the insertion procedure for both, w_∞ and τ , up to three-loop order. One obtains in both cases the same diagrams with the same fore-factors. The result is listed in Fig. 1.

APPENDIX D: EVALUATION OF DIAGRAMS FOR THE BACKBONE

In this appendix we give some details of the calculation of the backbone dimension. As described in Sec. IV C, we insert $\frac{1}{2}\phi^2$ into each conducting propagator. The diagram A for example has two conducting propagators. Its contribution to $Z_{w_{-1}}$ can be expressed as

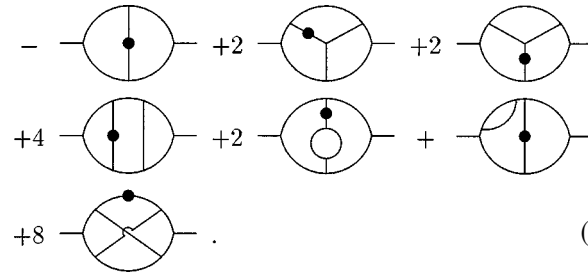

(D1)

As in Appendix C, the lines stand for conducting propagators evaluated at zero currents and the solid dot for a $\frac{1}{2}\phi^2$ -insertion. The diagram B contributes via

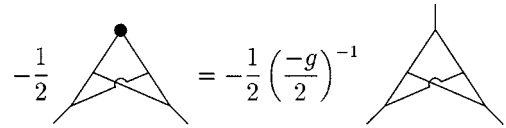

(D2)

and hence the total contribution of A-2B vanishes.

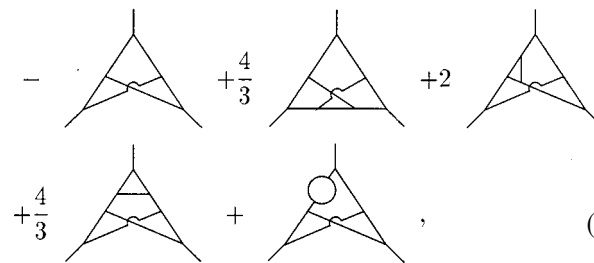
The procedure is carried out up to three-loop order. It results in


(D3)

These diagrams can be most conveniently evaluated by mapping them onto those calculated in Ref. [15]. The two-loop contribution for example can be reexpressed as


(D4)

Note that we have explicitly extracted the combinatorial factor $\frac{1}{2}$ from the diagram. This is important at this stage, since different diagrams, each inheriting its combinatorial factor from its bold diagram, may be mapped onto the same three-leg diagram. The additional factor on the right-hand side cancels the combinatorial factor $\frac{1}{2}$ of the three-leg diagram as well as a vertex $-g$. Similar identifications can be made for the three-loop diagrams appearing in Eq. (D3). After all, the following diagrammatic contributions to the renormalization of w_{-1} are obtained:


(D5)

where we have dropped an overall factor $-g^{-1}$.

The ϵ -expansion results for the diagrams in Eq. (D5) can be gathered from Ref. [15]. However, we did not entirely rely on the results stated there. We also did the calculations on our own and found the same results leading to the renormalization factor given in Eq. (4.24).

[1] A. Bunde and S. Havlin, *Fractals and Disordered Systems* (Springer, Berlin, 1991).
 [2] D. Stauffer and A. Aharony, *Introduction to Percolation Theory* (Taylor & Francis, London, 1992).
 [3] B. D. Hughes, *Random Walks and Random Environments* (Clarendon, Oxford, 1995).
 [4] H. K. Janssen, O. Stenull, and K. Oerding, *Phys. Rev. E* **59**,

R6239 (1999).
 [5] M. J. Stephen, *Phys. Rev. B* **17**, 4444 (1978).
 [6] A. B. Harris and T. C. Lubensky, *J. Phys. A* **17**, L609 (1984).
 [7] A. B. Harris, *Phys. Rev. B* **35**, 5056 (1987).
 [8] O. Stenull, H. K. Janssen, and K. Oerding, *Phys. Rev. E* **59**, 4919 (1999).
 [9] A. B. Harris and R. Fisch, *Phys. Rev. Lett.* **38**, 796 (1977).

- [10] C. Dasgupta, A. B. Harris, and T. C. Lubensky, *Phys. Rev. B* **17**, 1375 (1978).
- [11] S. W. Kenkel and J. P. Straley, *Phys. Rev. Lett.* **49**, 767 (1982).
- [12] R. Blumenfeld and A. Aharony, *J. Phys. A* **18**, L443 (1985).
- [13] See, e.g., R. K. P. Zia and D. J. Wallace, *J. Phys. A* **8**, 1495 (1975).
- [14] See, e.g., D. J. Amit, *Field Theory, the Renormalization Group, and Critical Phenomena* (World Scientific, Singapore, 1984); J. Zinn-Justin, *Quantum Field Theory and Critical Phenomena* (Clarendon, Oxford, 1989).
- [15] O. F. de Alcantara Bonfim, J. E. Kirkham, and A. J. McKane, *J. Phys. A* **13**, L247 (1980); **14**, 2391 (1981).
- [16] A. Coniglio, *Phys. Rev. Lett.* **46**, 250 (1981).
- [17] A. Coniglio, *J. Phys. A* **15**, 3829 (1982).
- [18] H. K. Janssen, *Z. Phys. B: Condens. Matter* **58**, 311 (1985); to first order in ϵ this result was also obtained by J. Cardy and P. Grassberger, *J. Phys. A* **18**, L267 (1985).
- [19] P. Grassberger, *J. Phys. A* **25**, 5867 (1992); e-print cond-mat/9906309 (unpublished).
- [20] A. B. Harris and T. C. Lubensky, *J. Phys. A* **6**, L365 (1983); A. B. Harris, *Phys. Rev. B* **28**, 2614 (1983).
- [21] P. Grassberger, *Physica A* **262**, 251 (1999).
- [22] C. Moukarzel, *Int. J. Mod. Phys. C* **8**, 887 (1998).
- [23] M. P. M. den Nijs, *J. Phys. A* **12**, 1857 (1979).
- [24] B. Nienhuis, *J. Phys. A* **15**, 199 (1982).
- [25] R. M. Ziff and G. Stell (unpublished); P. N. Strenski, R. M. Bradley, and J.-M. Debierre, *Phys. Rev. Lett.* **66**, 1330 (1991).
- [26] Y. Park, A. B. Harris, and T. C. Lubensky, *Phys. Rev. B* **35**, 5048 (1987).